Supporting Information

Visualizing Supramolecular Assembly Behavior, Stimulus Response, and Solid State Emission of Higher-Order Pt^{2+} Aggregates

Jing Li[1,2,§], Bao-Sen Xu[1,2,§], Shao-Zhe Yi[3,§], Xing-Long Zhang[1,2], Le-Le Zhao[1,2], Yu Meng[1,2], Wen-Jin Wang[4], Bao-Ning Li[1,2,3]*

[1]School of Chemistry and Chemical Engineering, Yulin University, Yulin 719000, People's Republic of China
[2]Shaanxi Key Laboratory of Low Metamorpcoal Clean Utilizationhic, Yulin University, Yulin 719000 , People's Republic of China
[3]Lehn Institute of Functional Materials, School of Chemistry, Sun Yat-Sen University, Guangzhou 510275, People's Republic of China
[4]Shenzhen Second Affiliated Hospital, Chinese University of Hong Kong, Shenzhen 518000, People's Republic of China

E-mail: lbning@yulinu.edu.cn

Instrumentation

NMR spectra were recorded on a Bruker DPX 400 FT–NMR spectrometer 400 MHz. Electrospray ionization mass spectra (ESI−MS) was performed on a Bruker Maxis 4G ESI–Q–TOF Bruker in MeCN solution. Elemental analyses of the complex were performed on a Vario EL elemental analyzer. Electronic absorption spectra in the UV−visible region were recorded with a Shimadzu UV−3600 spectrophotometer, in a 10×1 mm or 10×10 mm quartz cell. The photoluminescence spectra were measured on Edinburgh Instruments FS 980 and FS 5. Time-dependent single-photon counting technology (picosecond to microsecond) and multi-channel scanning technology (microsecond to second) were used for decay lifetime acquisition, using FLS 980

fluorescence spectrophotometer with 405 nm laser light source. The quantum yields (QYs) were measured using a Hamamatsu C9920-02G absolute photoluminescence quantum yield (PLQY) measurement system. Transmission electron micrographs (TEM) were recorded on a FEI Tecnai G2 Spirit system. The samples for TEM were prepared by dropcasting solutions on the ultrathin pure carbon film. Scanning electron microscope (SEM) experiments were performed by using field emission scanning electron microscopy (FESEM, Hitachi, SU8010) operating at an electron acceleration energy of 1 kV and 10 μA. The elemental mapping images were examined using the Zeiss Sigma300 electron scanning microscope. The SEM samples were prepared by dropping solutions onto a silicon wafer and dried naturally. Infrared spectra analysis was recorded on a Nicolet Nagna−IR 550 spectrophotometer in the region 4000−400 cm^{-1} using KBr pellets. Single-crystal diffraction data of organplatinum(II) complex was collected on an Agilent SuperNova X-ray diffractometer using micro-focus dual with X-ray Source of Cu-Kα radiation (λ = 1.54178 Å), respectively. All confocal images were taken with a Carl Zeiss LSM 880 laser scanning confocal microscope (Germany) combined with a Becker-Hickl time-correlated single photon counting system.

Experimental Section

Crystal structure determination of complex 1 and Ref-Pt

Single-crystal diffraction data of platinum(II) complex **1** and Ref-Pt was collected on an Agilent SuperNova X-ray diffractometer using micro-focus dual with X-ray Source of Cu–Kα radiation (λ = 1.54178 Å). Using Olex2[1], the structures were solved by

SHELXT[2] and refined using the full-matrix least-squares procedures within the SHELXTL software package refinement package using least squares minimization. CCDC 2045564 and 2075404, respectively, containing the supplementary crystallographic data for organplatinum(II) complex **1** and Ref-Pt, respectively, it can be obtained free of charge from the Cambridge Crystallographic Data Centre via www.ccdc.cam.ac.uk/data_request/cif.

Temperature-dependent isodesmic model in curve fitting of complex

Isodesmic model[3-4] developed by Meijer and coworkers have been applied to fit the experimental data in the variable temperature UV−vis spectroscopic studies in MeCN–H_2O mixtures. A cooling rate of 0.5 K min^{-1} was employed to keep the aggregation process under thermal equilibrium and thermodynamic control. The self-assembly process is undergoing isodesmic growth mechanism if every monomer addition to the supramolecular polymer is governed by a single equilibrium constant K_e. It is also known as the equal-K model[5-6]. In an isodesmic mechanism, the degree of aggregation, α, is related to temperature T by equation (1) below:

$$\alpha(T) = \frac{1}{1 + exp\left[-0.908\Delta H \frac{T - T_m}{RT_m^2}\right]} \quad (1)$$

T_m is the melting temperature defined as the temperature when $\alpha = 0.5$, while the molar enthalpy release (ΔH) is related to the formation of non-covalent interactions during the aggregation process. R is the universal gas constant. The above equation could be utilized to fit the experimental data obtained from the UV−vis absorption change at different temperature such that ΔH and T_m could be obtained. Furthermore, the average

stack length (DP_N) as well as the equilibrium constant (K_e) can be obtained, with concentration (c), by the equation (2) below:

$$DP_N = \frac{1}{\sqrt{1-\alpha(T)}} = \frac{1}{2} + \frac{1}{2}\sqrt{4K_e(T)c+1} \quad (2)$$

Calculations

To gain further insight into the photophysical and electrochemical characteristics of the Pt(II)-complex, theoretical studies on the electronic structures were carried out using density functional theory (DFT) and time-dependent DFT (TD-DFT) methods. The molecular structure was optimized at the ground state (S_0) in the gas phase. DFT calculations were conducted with the popular PBE0 functional theory and def2-SVP basis set. The excited states' energies of the Pt(II)-complex were computed by TD-DFT based on all the ground-state (S_0) geometries. Additionally, the natural transition orbital (NTO) was analyzed for $S_0 \rightarrow T_1$ excitation based on the first triplet state (T_1) geometries optimized by UPBE0. All calculations were carried out with Gaussian 09, Revision D.01 software package.

Materials

All starting materials were purchased from commercial sources and used as received, and the solvents used for synthesis were of analytical grade, unless stated otherwise. Complex [Pt(L)Cl] (N^CH^N = 2,2'(4,6-dimethyl-1,3-phenylene)-bipyridine) (dmpdpy) was prepared according to literature methods[7].

Synthesis of the complex 1

[Pt(L)Cl] (50 mg, 0.11 mmol) and $AgNO_3$ (26 mg, 0.15 mmol) are dissolved in in CH_2Cl_2 and MeOH mixed solution, and stirred for 30 min. Then filtering and addition of CH_3CN solvent, keep stirring 2 h, the resultant yellow solid is gradually precipitated, washed with excess amount of H_2O, ice MeOH and Et_2O, then recrystallized by slow diffusion of Et_2O into a concentrated CH_3CN solution. Pure product of complex **1** is isolated as dark red crystals. Yield: 53 %. ^{1}H NMR (400 MHz, CD_3CN, 298 K, relative

to Me_4Si, δ / ppm): ^1H NMR (400 MHz, CD_3CN): δ 8.01 (d, J = 4.7 Hz, 2H, −pyridine), 7.63 (t, J = 7.2, 3.9 Hz, 2H, −pyridine), 7.34 (d, J = 8.2 Hz, 2H, −pyridine), 6.87 (t, J = 7.9, 3.9 Hz,2H, −pyridine), 6.33 (s, 1H, −phenyl), 2.06 (s, 6H, -CH_3), 1.61 (s, 3H, -CH_3). ESI−MS: m/z : 495.1145 $[M]^+$, 454.0879 [M−MeCN]$^+$. Elemental analysis calcd (%) for $C_{84}H_{78}N_{22}O_{24}Ag_2Pt_4$: C 36.27, H 2.13, N 11.31; found: C 36.35, H 2.83, N 11.101. IR (KBr): v = 2174 (−C≡N) cm^{-1}, v = 1772 (NO_3^-) cm^{-1}.

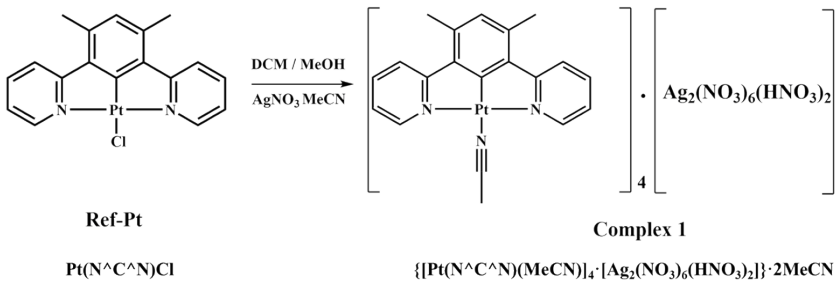

Scheme S1 Synthesis of organplatinum(II) complex **1**. (MeCN solvent is removed in the chemical structure.)

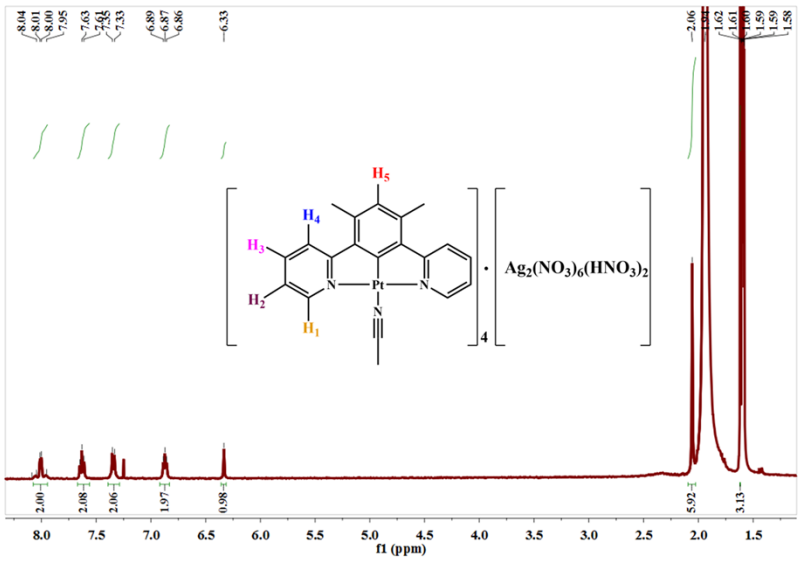

Figure S1 ^1H−NMR spectra organplatinum(II) complex **1** in CD_3CN solution. (MeCN solvent is removed in the chemical structure.)

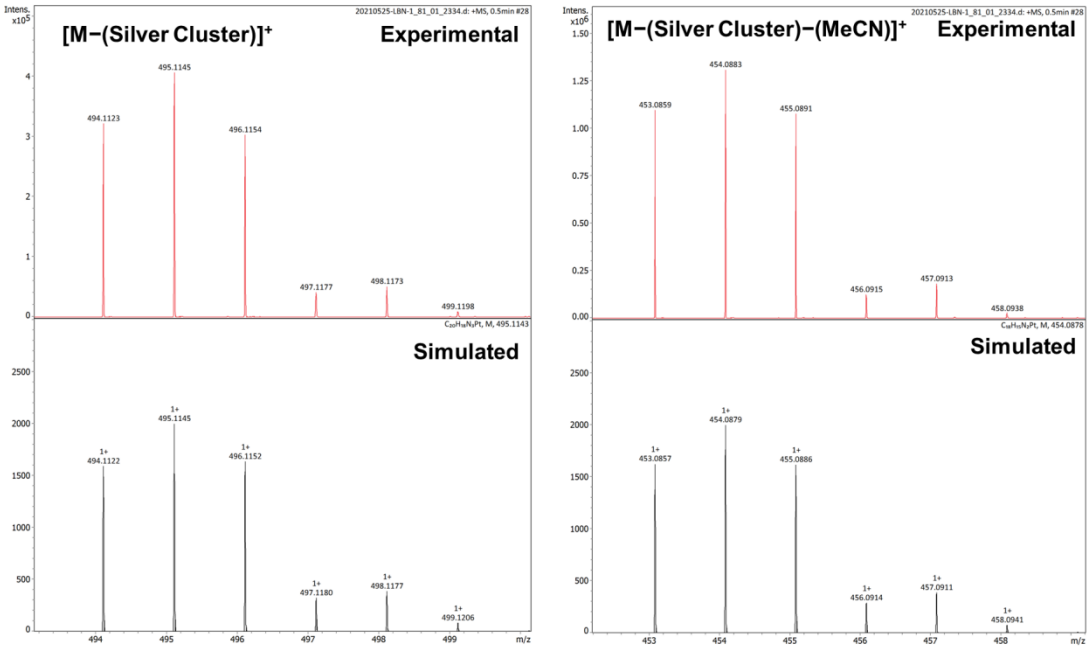

Figure S2 ESI−MS spectra of platinum(II) complex **1.**

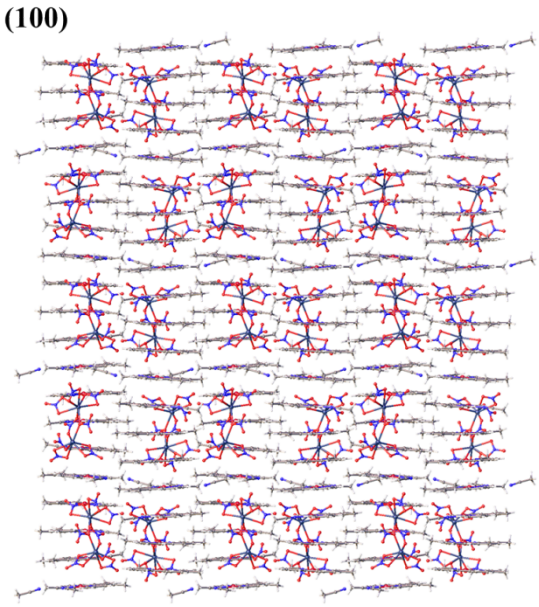

Figure S3 Molecular stacking to form extensive networks of platinum(II) complex **1** along the *a* axis.

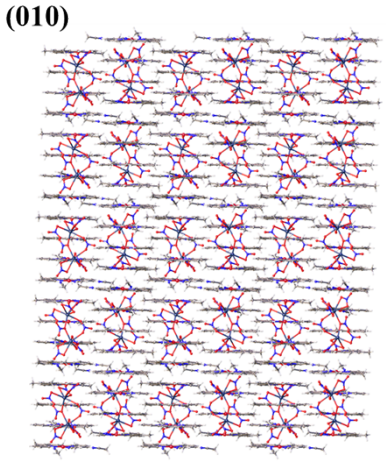

Figure S4 Molecular stacking to form extensive networks of platinum(II) complex **1** along the *b* axis.

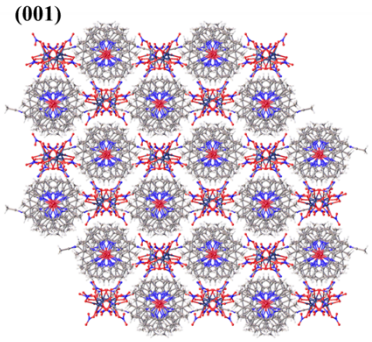

Figure S5 Molecular stacking to form extensive networks of platinum(II) complex **1** along the *c* axis.

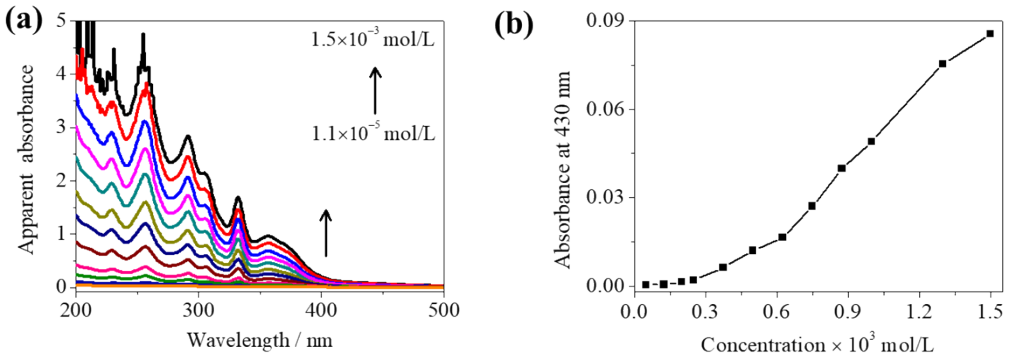

Figure S6 Concentration-dependent (a) UV−vis absorption of the complex **1** ranged from the concentration 10^{-5} to 10^{-3} M in MeCN solutions. (b) A plot of absorbance at 420 nm as a function of concentration of **1**.

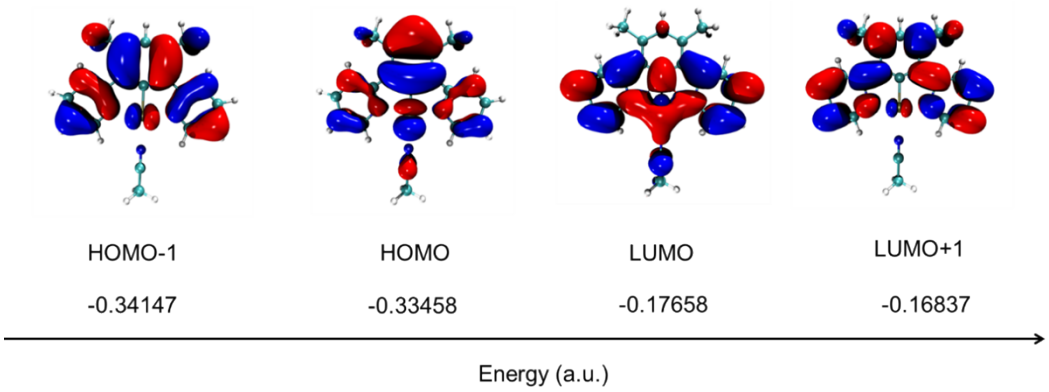

Figure S7 The HOMOs and LUMOs patterns for the Pt(II)-complex based on the optimized S_0 geometry.

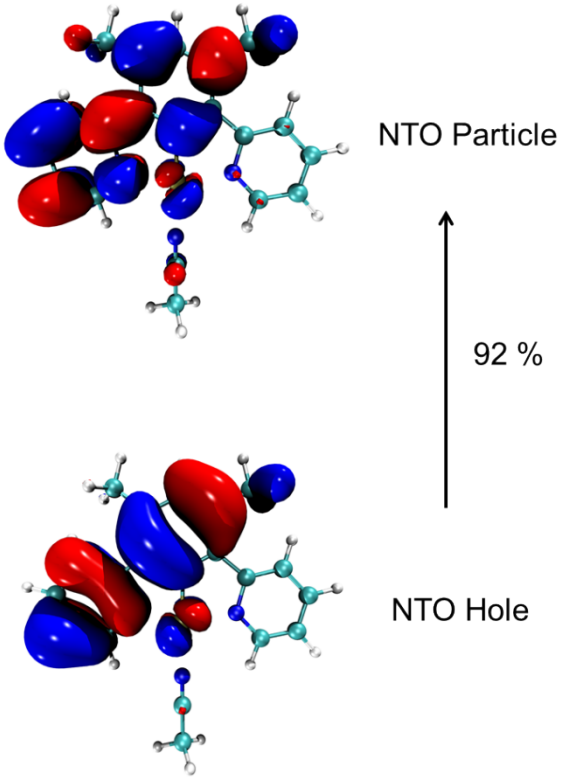

Figure S8 The NTO patterns for $S_0 \rightarrow T_1$ excitation for the Pt(II)-complex based on the optimized T_1 geometry.

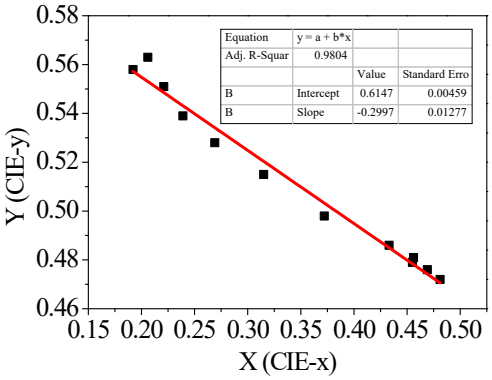

Figure S9 The linear fitting graph of the chromaticity coordinates dependent on the concentration. The equation (y = 0.6147−0.2997x) was established for the CIE coordinates.

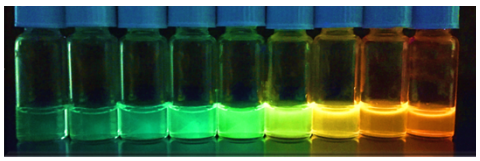

Figure S10 Corresponding photographs show the dramatic color change in the luminescent responses of **1** at UV light.

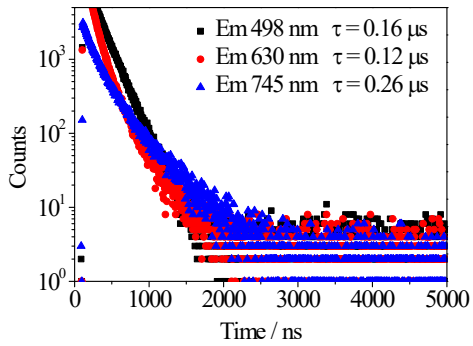

Figure S11 Lifetime spectra of the complex **1** in degassed MeCN solution under 298K.

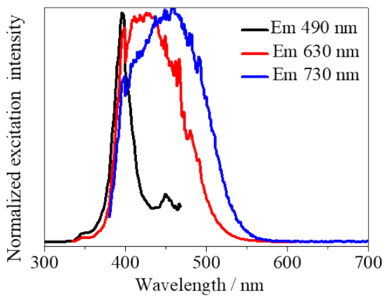

Figure S12 Normalized excitation sepctrum of complex **1** in degassed MeCN solution under 298K.

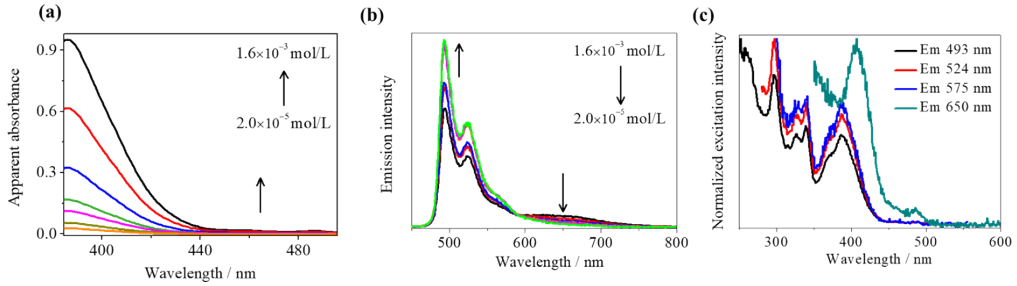

Figure S13 UV−vis spectra of complex Ref-Pt. (b) Emission spectra of Ref-Pt (with 455 nm filter). (c) Excitation spectra of Ref-Pt dependent on the concentrations in degassed dichloromethane soloution from 10^{-5} to 10^{-3} M at 298K.

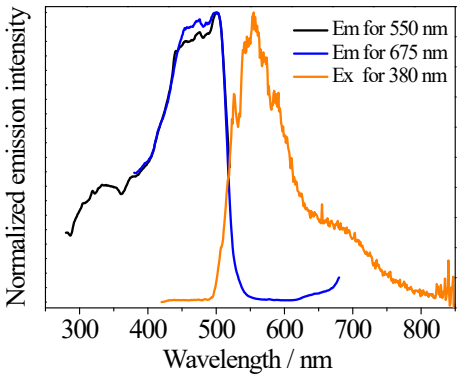

Figure S14 Emission spectra of Ref-Pt in solid state at 298K.

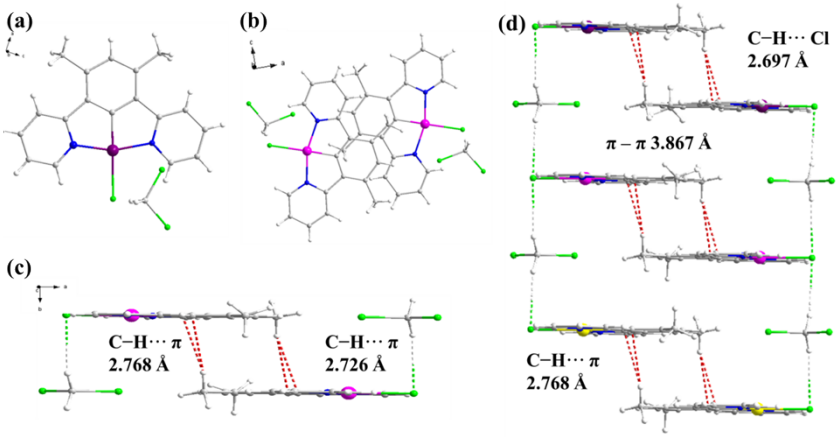

Figure S15 (a) Views of the crystal structure of chloroplatinum(II) complex precursors Ref-Pt, **(**b) viewed down onto the top of the dimer; (c) a side-on view of the dimer diagram, (d) Crystal packing diagrams of the Ref-Pt complex precursors.

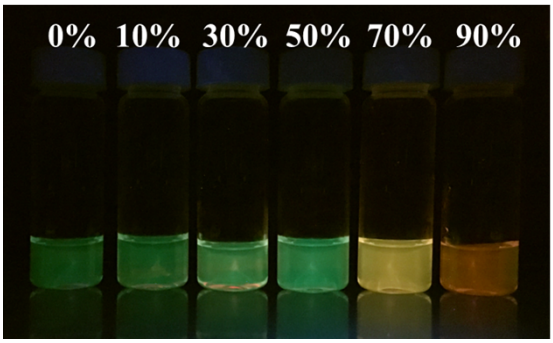

Figure S16 Photographs of **1** under 365 nm irradiation with increasing water content in MeCN solution at RT.

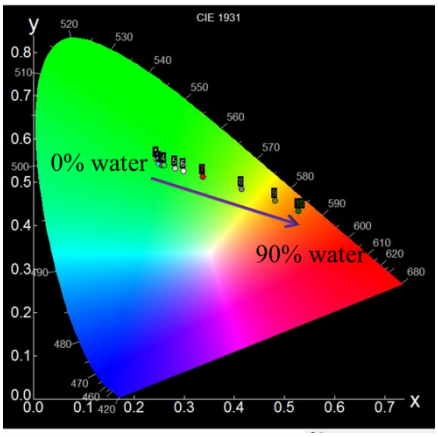

Figure S17 Corresponding CIE graph of complex **1** at different water portion in MeCN solution at the concentration of 1.0×10^{-5} M (λ_{ex} = 380 nm).

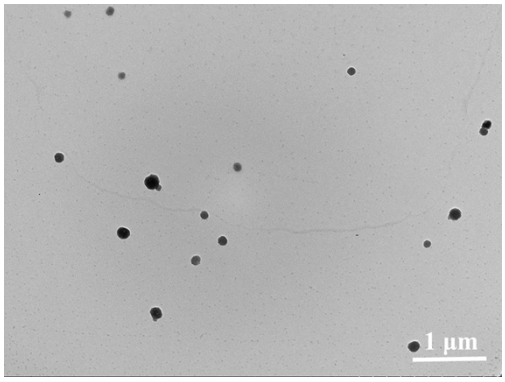

Figure S18 TEM image **1** prepared from MeCN solution at the concentration of 10^{-5} M.

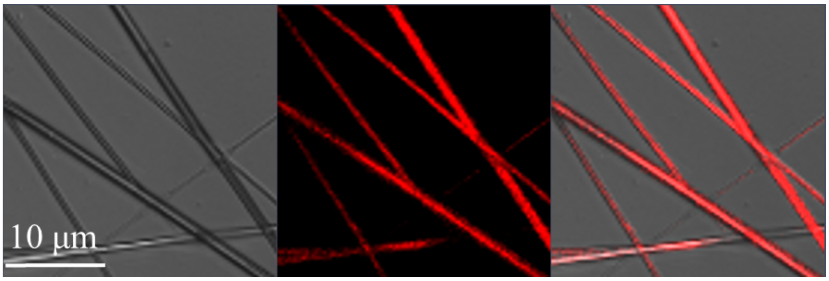

Figure S19 Confocal images **1** prepared from 90% water/MeCN mixture solutions at the concentration of 10^{-5} M.

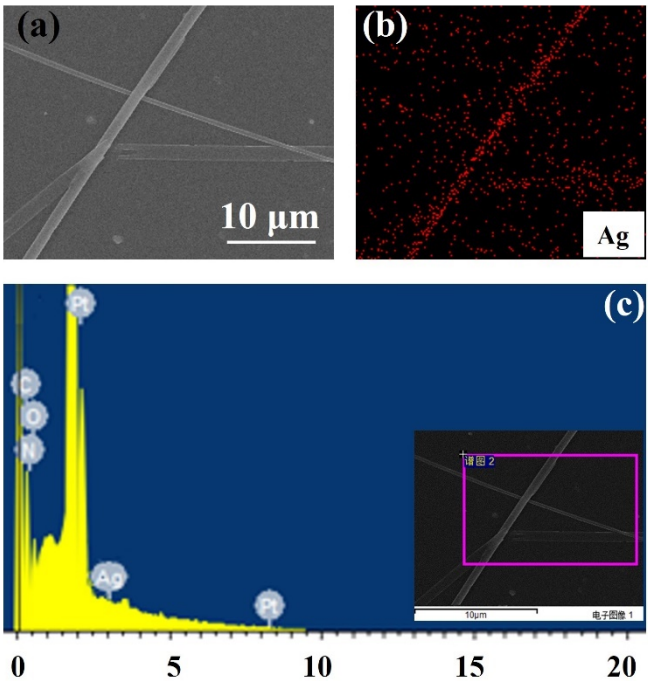

Figure S20 (a) SEM images of **1** were obtained from a 90% water/MeCN mixture with a concentration of 1.0×10−5 M. (b) Elemental mapping of Ag was performed to correlate with the SEM images. (c) The elemental distribution map was generated using point scanning methodology (inset: the selected area).

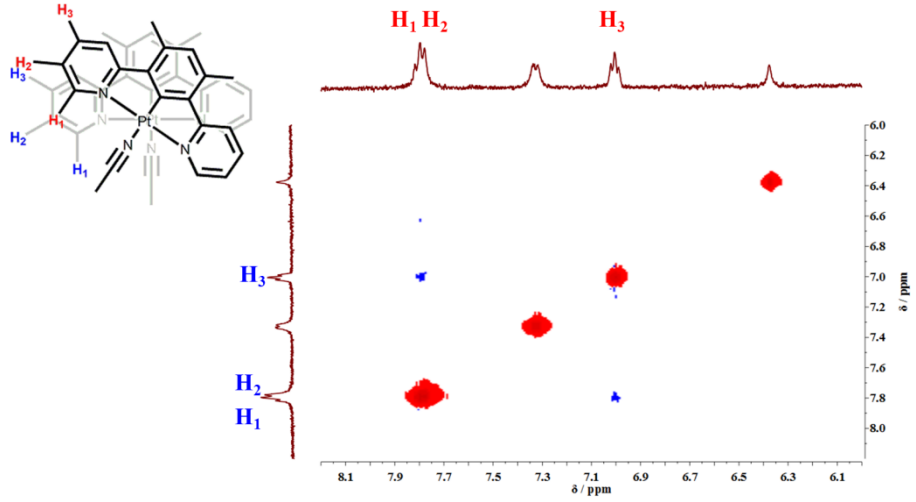

Figure S21 Partial ^{1}H NMR-NOESY spectra of complex **1** (10^{-4} M) in the mixture solution of [D_3]MeCN / D_2O = 1:9.

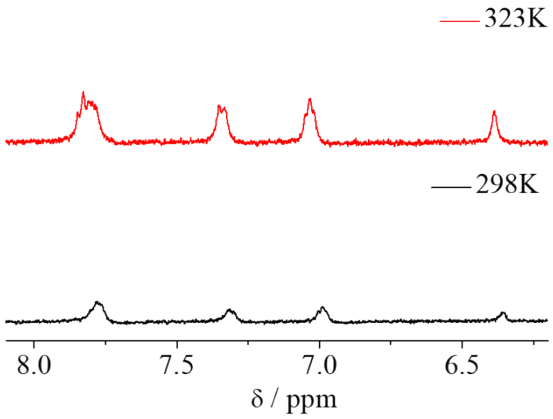

Figure S22 Temperature-dependent of the partial ^{1}H NMR spectra of complex **1** (10^{-4} M) in the mixture solution of [D_3]MeCN / D_2O = 1:9.

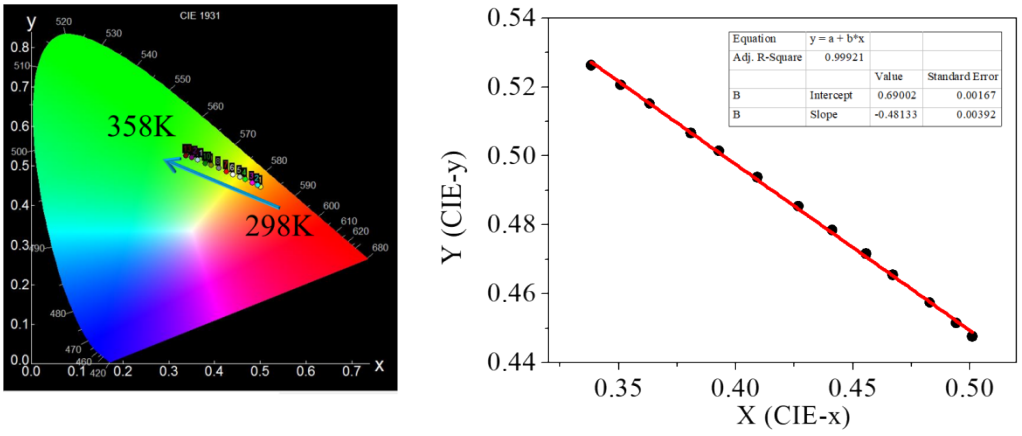

Figure S23 The linear fitting graph of the chromaticity coordinates dependent on the

temperature in (MeCN−water 20:80, v/v, 10^{-4} M) mixture solution. The equation (y = 0.6900−0.4813x) was established for the CIE coordinates.

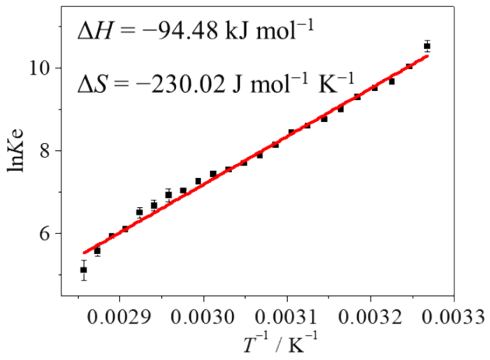

Figure S24 Van't Hoff plot of the equilibrium constant *K*e at various temperatures with the corresponding thermodynamic parameters.

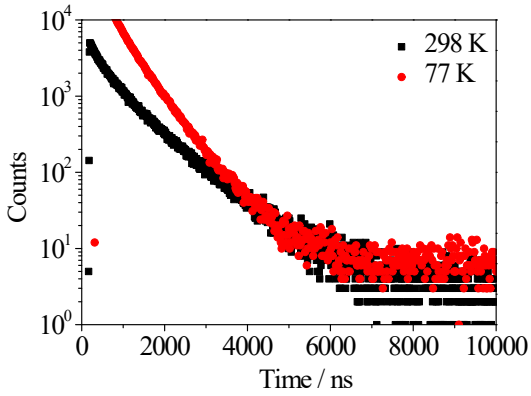

Figure S25 Dependent lifetime spectra of complex **1** in solid state.

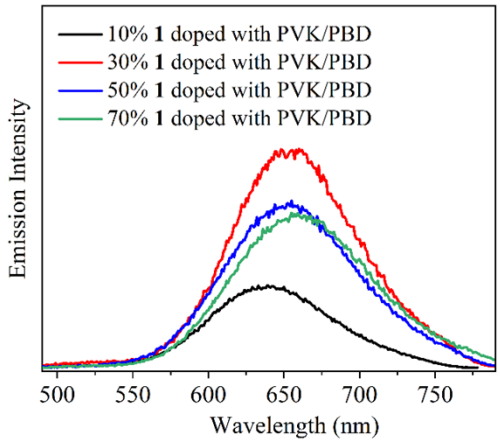

Figure S26 The photoluminescence diagram for different doping ratios between PVK /PBD and complex **1**.

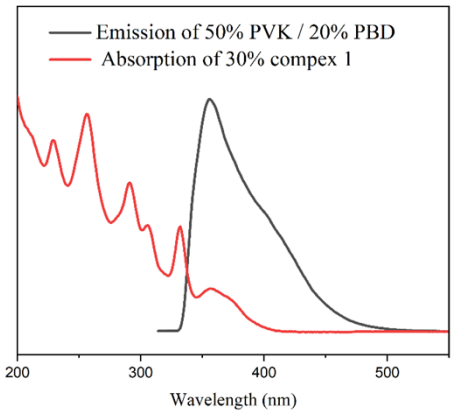

Figure S27 The comparison diagram between the emission of PVK and PBD mixed and the absorption of complex **1**.

Table S1 Crystal data and structure refinement for complex **1** and Ref-Pt.

Complexes	**1**	Ref-Pt
Empirical formula	$C_{84}H_{78}Ag_2N_{22}O_{24}Pt_4$ (+solvent)	$C_{19}H_{17}Cl_3N_2Pt$ (+solvent)
Formula weight	2775.78	574.78
Temperature/K	250.00(10)	240.00(10)
Crystal system	*monoclinic*	monoclinic
Space group	*P21/c*	$P2_1/m$
a/Å	17.6693(2)	16.1259(4)
b/Å	18.7992(2)	6.8629(2)
c/Å	27.1249(3)	16.8334(4)
α/°	90	90
β/°	92.0790(10)	90.667(2)
γ/°	90	90
Volume/Å^3	9004.11(17)	1862.83(8)
Z	4	4
ρ g/cm^3	2.048	2.049
μ/mm^{-1}	15.491	18.077
F(000)	5336	1096
Reflections collected	31901	6563
Data/restraints/parameters	16939/802/1101	3892/0/303
Goodness-of-fit on F^2	1.435	1.053
Final *R* indexes [$I \geq 2\sigma(I)$]	R_1 = 0.1012, wR_2 = 0.3140	R_1= 0.0553, wR_2= 0.1563
Final *R* indexes [all data]	R_1 = 0.1143, wR_2 = 0.3422	R_1= 0.0580, wR_2= 0.1607
Largest diff. peak/hole / e Å^{-3}	9.10/-7.41	2.99/-3.15

Table S2 Selected bond lengths (Å) for complex **1** and Ref-Pt.

1		Ref-Pt	
N11 Pt1 N13	100.5(6)	N1 Pt1 Cl5	97.8(3)
N12 Pt1 N11	162.1(6)	N2 Pt1 Cl5	99.7(2)
N12 Pt1 N13	97.4(5)	N2 Pt1 N1	162.5(4)
C13 Pt1 N11	79.5(6)	C13 Pt1 Cl5	179.7(3)
C13 Pt1 N12	82.6(6)	C13 Pt1 N1	81.9(4)
C13 Pt1 N13	179.2(5)	C13 Pt1 N2	80.6(4)

Table S3 Selected bond angles (°) for complex **1** and Ref-Pt.

1			Ref-Pt		
Pt1	N11	2.016(15)	Pt1	Cl5	2.431(2)
Pt1	N12	2.008(14)	Pt1	N1	2.018(9)
Pt1	N13	2.098(15)	Pt1	N2	2.009(8)
Pt1	C13	1.911(13)	Pt1	C13	1.912(10)

Table S4 Photophysical data for complex **1**.

Complex	**Medium**	**Electronic absorption**	**Emission**	**QY_{PL}[#]**
	T/K	(ε [$dm^3mol^{-1}cm^{-1}$]) (10^{-5})	(τ [μs])	
1	MeCN (298)	233 (6810), 259 (7370), 290 (5125), 305 (3395), 332 (3020), 360 (1435)	494 (3.12) 521	0.028
	Solid (298)	-	650 (0.77)	0.127
	Solid (77)	-	710 (1.27)	-

[-] Not measured. [#] The emission quantum yields were the maximum value under different excitation measured on a Hamamatsu C9920-02G absolute PL quantum yield measurement system.

Table S5 The TD-DFT results for chiral Pt(II)-complex based on their optimized S_0 geometries.

MO	Contribn of metal dπ and π orbitals of ligand to MOs (%)			Main confign of $S_0 \rightarrow S_n$ excitation, λ_{cal}(nm)/f [a]	Main confign of $S_0 \rightarrow T_1$ excitation, λ_{cal}(nm)[a]
	Pt	Lig	Ace		
L+1	1.51	98.49	0	S_1: H→L (96.6), 362.6, 0.0011	H→L (73.6), H→L+1 (9.6), H-1→L+1 (8.3), 597.7
L	7.00	89.10	3.90		
H	20.09	78.10	1.46	S_2: H-1 → L (94.9), 352.4, 0.0086	
H-1	7.30	92.27	0		
				S_3: H→ L+1 (93.0), 342.2, 0.1240	

[a]H→ L denotes the transition from HOMO to LUMO. λ_{cal}, and *f* denote the calculated emission wavelength, and oscillator strength, respectively. The oscillator strength of $S_0 \rightarrow T_1$ is zero owing to the spin-forbidden character of the singlet-triplet transition under TD-DFT calculations in the Gaussian program with no consideration of spinorbital coupling.

Table S6 The NTO results for the Pt(II)-complex based on the optimized T_1 geometry.
NTO calculations for S_0 - T_1 excitations indicated that about 96% of the hole orbital was contributed by and 90% of the particle orbital was from the ligand for the Pt(II) complex, forming almost the entire (ca. 92%) hole - particle transition.

NTO [a]	Contribn of metal dπ and π orbitals of ligand to MOs (%)		
	Pt	Lig	Ace
H	4.11	95.65	0.24
P	9.81	89.67	0.52

[a]H and P denote NTO hole and particle orbitals, respectively

Table S7 Thermodynamic parameters for self-assembly of complex **1**.

Complex	ΔH / kJ mol^{-1}	T_m [a] / K	K_e [a] / L mol^{-1}	ΔS [b] / J mol^{-1}K^{-1}	ΔG [b] / kJ mol^{-1}	DP_N
1	−79.21[a] −94.48[b]	315.76	5.25×10^3	−230.02	−21.84	1.60

a: Determined by the fitting curve of the degree of aggregation against temperature according to the temperature-dependent isodesmic model. *b*: Determined by the Van't Hoff plot from the temperature-dependent UV-vis absorption spectra.

Table S8 CIE of the complex **1** dependent on the concentration, solvent and temperature when excited at $\lambda_{ex} = 380$ nm.

Concentration		Solvent		Temperature	
CIE (x, y)		CIE (x, y)		CIE (x, y)	
0.481	0.472	0.501	0.448	0.246	0.553
0.469	0.476	0.494	0.451	0.251	0.543
0.456	0.481	0.483	0.457	0.258	0.540
0.455	0.479	0.467	0.465	0.261	0.539
0.433	0.486	0.456	0.472	0.282	0.531
0.372	0.498	0.441	0.478	0.299	0.526
0.315	0.515	0.427	0.485	0.338	0.512
0.269	0.528	0.409	0.494	0.416	0.483
0.239	0.539	0.393	0.501	0.482	0.458
0.221	0.551	0.381	0.507	0.528	0.434
0.206	0.563	0.363	0.515		
0.192	0.558	0.351	0.521		
		0.338	0.526		

REFERENCES

1. Dolomanov, O. V.; Bourhis, L. J.; Gildea, R. J.; Howard, J. A. K.; Puschmann, H., OLEX2: A Complete Structure Solution, Refinement and Analysis program. *J. Appl. Crystallogr.* **2009,** *42*, 339-341.
2. Sheldrick, G., J Acta Crystallographica Section A, A short history of SHELX. **2008,** *64*, 112-122.
3. Jonkheijm, P.; van der Schoot, P.; Schenning, A. P.; Meijer, E. W., Probing the Solvent-Assisted Nucleation Pathway in Chemical Self-Assembly. *Science* **2006,** *313*, 80-83.
4. Korevaar, P. A.; Schaefer, C.; de Greef, T. F.; Meijer, E. W., Controlling Chemical Self-Assembly by Solvent-Dependent Dynamics. *J. Am. Chem. Soc.* **2012,** *134*, 13482-13491.
5. Chan, M. H.-Y.; Leung, S. Y.-L.; Yam, V. W.-W., Controlling Self-Assembly Mechanisms through Rational Molecular Design in Oligo(*p*-phenyleneethynylene)-Containing Alkynylplatinum(II) 2,6-Bis(N-alkylbenzimidazol-2'-yl)pyridine Amphiphiles. *J. Am. Chem. Soc.* **2018,** *140*, 7637-7646.
6. Smulders, M. M.; Nieuwenhuizen, M. M.; de Greef, T. F.; van der Schoot, P.; Schenning, A. P.; Meijer, E. W., How to Distinguish Isodesmic from Cooperative Supramolecular Polymerisation. *Chem. Eur. J.* **2010,** *16*, 362-367.
7. Schulze, B.; Friebe, C.; Jäger, M.; Görls, H.; Birckner, E.; Winter, A.; Schubert, U. S., Pt^{II} Phosphors with Click-Derived 1,2,3-Triazole-Containing Tridentate Chelates. *Organometallics* **2017,** *37*, 145-155.